Revisiting inward rectification: K ions permeate through Kir2.1 channels during high-affinity block by spermidine

Tai-An Liu, Hsueh-Kai Chang, and Ru-Chi Shieh

Institute of Biomedical Sciences, Academia Sinica, Taipei 11529, Taiwan

Outward currents through Kir2.1 channels play crucial roles in controlling the electrical properties of excitable cells, and such currents are subjected to voltage-dependent block by intracellular Mg^{2+} and polyamines that bind to both high- and low-affinity sites on the channels. Under physiological conditions, high-affinity block is saturated and yet outward Kir2.1 currents can still occur, implying that high-affinity polyamine block cannot completely eliminate outward Kir2.1 currents. However, the underlying molecular mechanism remains unknown. Here, we show that high-affinity spermidine block, rather than completely occluding the single-channel pore, induces a subconducting state in which conductance is 20% that of the fully open channel. In a D172N mutant lacking the high-affinity polyamine-binding site, spermidine does not induce such a substate. However, the kinetics for the transitions between the substate and zero-current state in wild-type channels is the same as that of low-affinity block in the D172N mutant, supporting the notion that these are identical molecular events. Thus, the residual outward current after high-affinity spermidine block is susceptible to low-affinity block, which determines the final amplitude of the outward current. This study provides a detailed insight into the mechanism underlying the emergence of outward Kir2.1 currents regulated by inward rectification attributed to high- and low-affinity polyamine blocks.

INTRODUCTION

Inward rectifier K^+ channels (Kir channels) are important in the maintenance of stable resting membrane potentials, in controlling excitability, and in shaping the final repolarization of action potentials in excitable cells (Noble, 1979; Constanti and Galvan, 1983; Hume and Uehara, 1985; Day et al., 2005). Outward Kir currents at voltages (V_m) near the K^+ reversal potential are only slightly smaller than the inward currents. As the voltage becomes more depolarized, the outward current deviates more from the ohmic conductance and finally becomes minimal. Thus, a plot of the outward I–V_m relationship rises to a maximum and then falls.

The unique hump shape of the Kir I–V_m relationship plot is attributed to the presence of an inward rectification mechanism, which allows inward current to pass through the channel more easily than is the case with outward current. The mechanism underlying inward rectification of Kir channels has been ascribed to be voltage-dependent block of outward current by internal Mg^{2+} and polyamines (Matsuda et al., 1987; Vandenberg, 1987; Ficker et al., 1994; Lopatin et al., 1994; Stanfield et al., 1994). Kir2.1 channels (Kubo et al., 1993) can be blocked by these molecules with either high or low affinity (Yang et al., 1995a; Kubo and Murata, 2001). However, the relative contribution of the high- and low-affinity blocks to the formation of the hump-shape I–V_m relationship was not investigated until 2004 (Ishihara and Ehara, 2004; Ishihara and Yan, 2007). It was shown

that the chord conductance (G)–V_m relationship of the Kir2.1 channel could be modeled as a sum of two Boltzmann relationships, wherein the major portion reflected high-affinity polyamine block and the minor portion the low-affinity block (Ishihara and Ehara, 2004). Furthermore, it was suggested that most outward Kir2.1 current was likely attributed to K^+ ions conducting through a small population of channels, in a state susceptible to low-affinity block under physiological conditions featuring saturation of the high-affinity component (Ishihara and Ehara, 2004; Ishihara and Yan, 2007). Therefore, the formation of outward currents, and the appearance of the hump-shape I–V_m relationship, may be explained by the idea that high-affinity block does not completely inhibit outward I_{K1}.

Two hypotheses have been proposed to explain the incompleteness of the high-affinity block. One suggests that such a block reduces but does not completely eliminate Kir2.1 channel function, until a second blocker binds to the same channel with lower affinity (as a result of the electrostatic repulsion and steric hindrance between the blockers) and completely occludes the channel pore (Yang et al., 1995b). The second hypothesis is that Kir2.1 channels may exist in two states susceptible to high- and low-affinity block, respectively, and that the channel has a higher probability of being present in

The Rockefeller University Press $30.00
J. Gen. Physiol. Vol. 139 No. 3   245–259
www.jgp.org/cgi/doi/10.1085/jgp.201110736

245

the former state (Ishihara and Ehara, 2004). In the present study, we tested these two competing hypotheses by studying outward single-channel currents. Our results show that K$^+$ ions can still permeate through single Kir2.1 channels during high-affinity spermidine block.

MATERIALS AND METHODS

Preparation of *Xenopus laevis* oocytes and molecular biology
Xenopus oocytes were isolated by partial ovariectomy of frogs anaesthetized with 0.1% (wt/vol) tricaine (3-aminobenzoic acid ethyl ester), as described previously (Chang et al., 2005). The surgery protocol was conducted in accordance with the Guide for the Care and Use of Laboratory Animals (1996. National Academy of Sciences, Washington, D.C.). Mouse Kir2.1 channels subcloned in pGEMHE vectors were provided by L. Jan (University of California, San Francisco, San Francisco, CA). D172N mutants were generated using polymerase chain reaction, and the correctness of mutation was confirmed by sequencing of cDNAs using an ABI Prism dRhodamine Terminator Cycle Sequencing Ready Reaction kit (Applied Biosystems). cRNAs were obtained by in vitro transcription (mMessage mMachine; Invitrogen) and were injected in *Xenopus* oocytes (60–125 ng for giant-patch experiments and 0.03–0.3 ng for single-channel recordings), which were used 1–3 d after cRNA injection.

Electrophysiological recordings
Currents were recorded at room temperature (21–24°C) using patch-clamp techniques (Hamill et al., 1981; Hilgemann, 1995). The extracellular solution (pH 7.4) contained (in mM): 148 KCl, 2 KOH, 5 HEPES, and 0.25 GdCl$_3$. The intracellular solution (pH 7.4) contained (in mM): 121 KCl, 20 KOH, 4 K$_2$HPO$_4$, 1 KH$_2$PO$_4$, and 5 EDTA. For selectivity experiments, the intracellular solution (pH 7.4) contained (in mM): 150 XNO$_3$ + XOH, 0.1 EDTA, and 5 HEPES (X = K, Na, or NH$_4$). The extracellular solution (pH 7.4) contained (in mM): 20 KNO$_3$ + KOH, 0.1 EDTA, 5 HEPES, and 0.25 GdCl$_3$. The sampling/filtering frequencies were 20 kHz/5 kHz for giant-patch recordings and 10 kHz/1 kHz for single-channel recordings. Command voltages were controlled by and data were acquired with pClamp10 software (Molecular Devices).

Data analysis
Open- and blocked-time distributions were best-fitted to one or two exponential equations, using the maximum likelihood method (Sigworth and Sine, 1987). To calculate mean single-channel current, leak current was first subtracted from the single-current trace. The area under the i-time curve was calculated by integration, and the mean single-channel current was obtained by dividing the area with the total recording time. Mean single-channel conductance was then obtained by dividing the mean current with the voltage at which the current was recorded. Averaged data are presented as means ± SEMs. Student's *t* test for independent samples was used to assess the statistical significance of differences. The normalized G–V$_m$ relationships were fitted to the following Boltzmann relationships:

$$G/G_{ctrl} = \frac{A_1}{1 + \exp[z_1 F(V - V_{h1})/RT]} + \frac{A_2}{1 + \exp[z_2 F(V - V_{h2})/RT]} + (1 - A_1 - A_2), \quad (1)$$

where A$_1$ and A$_2$ are the factional amplitudes of the first and second Boltzmann components; 1–A$_1$–A$_2$ is the fractional pedestal current that is sensitive to polyamine block in a voltage-independent

manner; V$_{h1}$ and V$_{h2}$ are the half-activation voltages; z$_1$ and z$_2$ are the effective valences of the high- and low-affinity blocks; and R, T, and F are the usual physical constants. To estimate the apparent dissociation constants (K$_1$ and K$_2$), chord conductance sensitive to high-affinity block (G$_1$) and low-affinity block (G$_2$) were calculated from the first and second term of Eq. 1, respectively. The dose dependence of G$_1$ and G$_2$ was then fitted to the Hill equation:

$$G_n = A_n / (1 + K_n / [\text{spermidine}]_i), \quad (2)$$

where $n = 1$ or 2.

Online supplemental material
The online supplemental material illustrates the O-S-B model, simulations with the O-S-B model, the fitting of data to Eq. 1 and the fitting parameters. It is available at http://www.jgp.org/cgi/content/full/jgp.201110736/DC1.

RESULTS

High- and low-affinity blocks produced by intracellular spermine and spermidine
It has been previously shown that G–V$_m$ relationships in the presence of intracellular polyamines display two components sensitive to high- and low-affinity inhibition (Ishihara and Ehara, 2004; Ishihara and Yan, 2007). We first repeated these experiments. Fig. 1 A shows macroscopic Kir2.1 currents recorded from inside-out patches perfused with a symmetrical 150-mM [K$^+$] solution in the absence (control) and presence of the indicated intracellular spermidine concentration, [spermidine]$_i$. 0.1–50 μM spermidine inhibited outward I$_{K1}$ in a time- and dose-dependent manner. Fig. 1 B shows the normalized steady-state I–V$_m$ relationships obtained at various [spermine]$_i$ (Fig. 1 B, a) and [spermidine]$_i$ (Fig. 1 B, b) as indicated. As in the previous study (Ishihara and Ehara, 2004), the steady-state I–V$_m$ relationship obtained at [spermine]$_i$ ≤ 0.1 μM showed two distinct peaks of outward Kir2.1 current. Fig. 1 C shows the normalized G–V$_m$ relationships obtained with the indicated [spermine]$_i$ (Fig. 1 C, a) and [spermidine]$_i$ (Fig. 1 C, b). The G–V$_m$ relationships in the presence of polyamines could be described by the sum of two Boltzmann relationships (Eq. 1) (Fig. 1 C, black lines), corresponding to high- and low-affinity inhibitions by polyamines, and a small pedestal component, 1–A$_1$–A$_2$ (see Eq. 1). Fig. 1 D shows that the fraction of conductance susceptible to high-affinity block (red line) was 93% with 0.01 μM [spermine]$_i$ and 80% with 0.1 μM [spermidine]$_i$, and the conductance susceptible to low-affinity block (green line) was 6% with spermine and 18% with spermidine. Fig. 1 E shows that the dissociation constants for the high- and low-affinity block decreased exponentially with increasingly depolarizing voltages. The voltage dependence of the high-affinity block was steeper than that of low-affinity block. These results were similar to those described previously (Ishihara and Ehara, 2004).

High-affinity block by spermidine induced a channel substate rather than completely eliminating single-channel conductance

Next, we examined outward single-channel currents in an attempt to identify which of the two aforementioned hypotheses might be correct. According to the incomplete high-affinity inhibition hypothesis, a high-affinity block will not completely eliminate the single-channel current. Scheme 1 is a simple model for transition of the Kir2.1 channel:

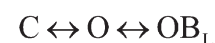$$C \leftrightarrow O \leftrightarrow OB_H \leftrightarrow OB_{HL}$$

(SCHEME 1)

where C is an intrinsic closed state, O a fully open state, OB_H a substate generated by incomplete inhibition of

the Kir2.1 channel by high-affinity block, and OB_{HL} the blocked state obtained when the Kir2.1 channel is subjected to both high- and low-affinity block. Fig. 1 D indicates that the ratios of maximum conductance in the O and OB_H states should be 15.3:1 with 0.01 µM $[spermine]_i$ and 4.4:1 with 0.1 µM $[spermidine]_i$. On the other hand, the two-state hypothesis predicts that both high- and low-affinity blocks would completely abolish outward single-channel current in the manner shown in Scheme 2:

State I. $\qquad C \leftrightarrow O \leftrightarrow OB_H$

State II. $\qquad C \leftrightarrow O \leftrightarrow OB_L$
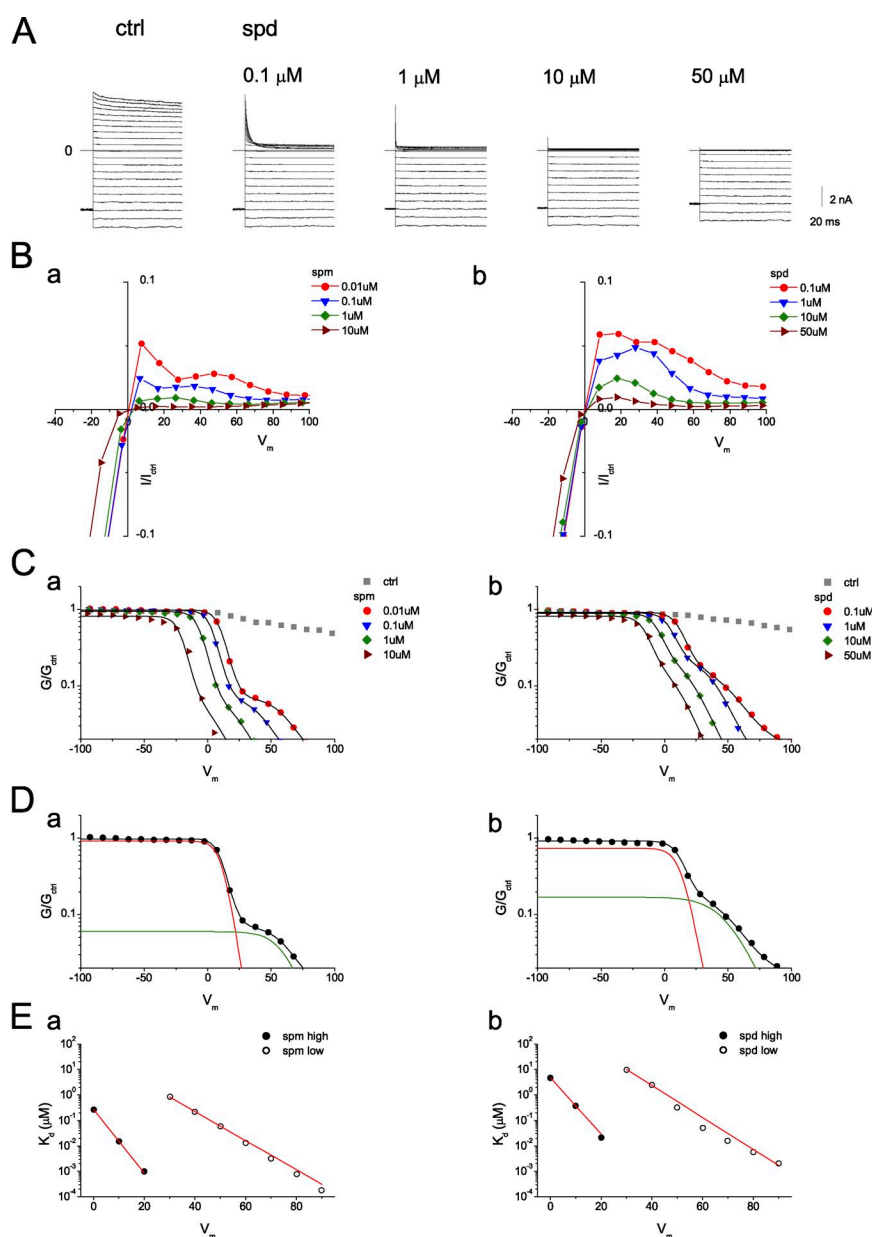
(SCHEME 2)

Figure 1. Inhibition of Kir2.1 channels by intracellular spermine and spermidine. (A) Current traces recorded from an inside-out giant patch in control and in the presence of the indicated concentrations of spermidine (spd). Currents were recorded from a holding potential of −80 mV, followed by test pulses (400 ms) in the range of −100 to +100 mV in 10-mV increments. (B) Normalized steady-state I–V_m relationships in the presence of spermine (a) and spermidine (b). Currents were normalized to that obtained at −100 mV in control. (C) Normalized G–V_m relationships shown on a semilogarithmic scale for the indicated $[spermine]_i$ (a) and $[spermidine]_i$ (b). Black lines show fits to Eq. 1. Fitting parameters are listed in Table S1. (D) Normalized G–V_m relationships obtained at 0.01 µM $[spermine]_i$ (a) and 0.1 µM $[spermidine]_i$ (b) were fit to Eq. 1. Red and green lines are the principal (high-affinity block) and minor (low-affinity block) Boltzmann components, respectively. (E) Voltage dependence of dissociation constants for high- and low-affinity block. Straight lines are fits with Eq. S2. For spermine block, $K_d(0) = 0.27$ µM and $z = 6.7$ for high-affinity block; $K_d(0) = 43$ µM and $z = 3.0$ for low-affinity block. For spermidine block, $K_d(0) = 4.8$ µM and $z = 5.9$ for high-affinity block; $K_d(0) = 782$ µM and $z = 3.3$ for low-affinity block.

where OB_L is the open-channel state with block by the low-affinity component, and the conductance of both the OB_H and OB_L states is zero. Fig. 1 D indicates that the ratios of state I to II would be 15.3:1 in the presence of 0.01 µM [spermine]$_i$ and 4.4:1 in the presence of [spermidine]$_i$.

If Scheme 1 is correct, substate conductance would be larger in the presence of spermidine than spermine. In addition, the high-affinity block was near-saturated at about +30 mV in the presence of 0.1 µM [spermidine]$_i$ (Fig. 1 D, b). When [spermidine]$_i$ increased, the high-affinity block became saturated at less depolarized voltages, and outward currents through Kir2.1 channels in this substate would thus be smaller (Fig. 1 C, b). Therefore, in this study, we chose 0.1 µM [spermidine]$_i$ for use in our experiments. Fig. 2 A shows a single-channel recording obtained at +40 mV in the presence of 150 mM of symmetrical [K$^+$]. In the absence of intracellular blockers (control), the channel stayed mainly at an open state (O) and a zero-current level (Fig. 2 A, closed state, C). Upon the addition of 0.1 µM [spermidine]$_i$, the channel mainly occupied a subconducting state (Fig. 2 A, substate, S). The open time was shortened, and the closed time was dominated by a short component (see Fig. 3 C). The substate was observed in all 100

examined patches containing the Kir2.1 channel treated with spermidine. Fig. 2 B shows single-channel currents recorded with voltage steps to +30, +50, and +70 mV under control conditions. The channel remained principally in the open state at +30 mV (Fig. 2 B, a). At more positive voltages, substates (denoted by S1–S3) of different levels were occasionally observed, in addition to the open and closed states (Fig. 2 B, b and c). Fig. 2 D shows the amplitude histogram of substates recorded at +40 mV under control conditions. The substate current amplitude ranged from 0.2 to 0.7 pA. In the presence of 0.1 µM [spermidine]$_i$, a single substate was observed at all three voltages, in addition to the zero-current (CB, closed and blocked states) and fully open states (Fig. 2 C). The amplitude of the substate induced by spermidine ranged from 0.08 to 0.4 pA at +40 mV (Fig. 2 D). These results suggest that the substate observed under control condition is not a result of residual spermidine block. The substates found in the control condition occurred infrequently and thus should not affect the analysis of the substate described below. At +30 mV, the channel transited principally between the open state and the substate (Fig. 2 C, a). The channel seldom transited from the substate to the zero-current state (such events are indicated
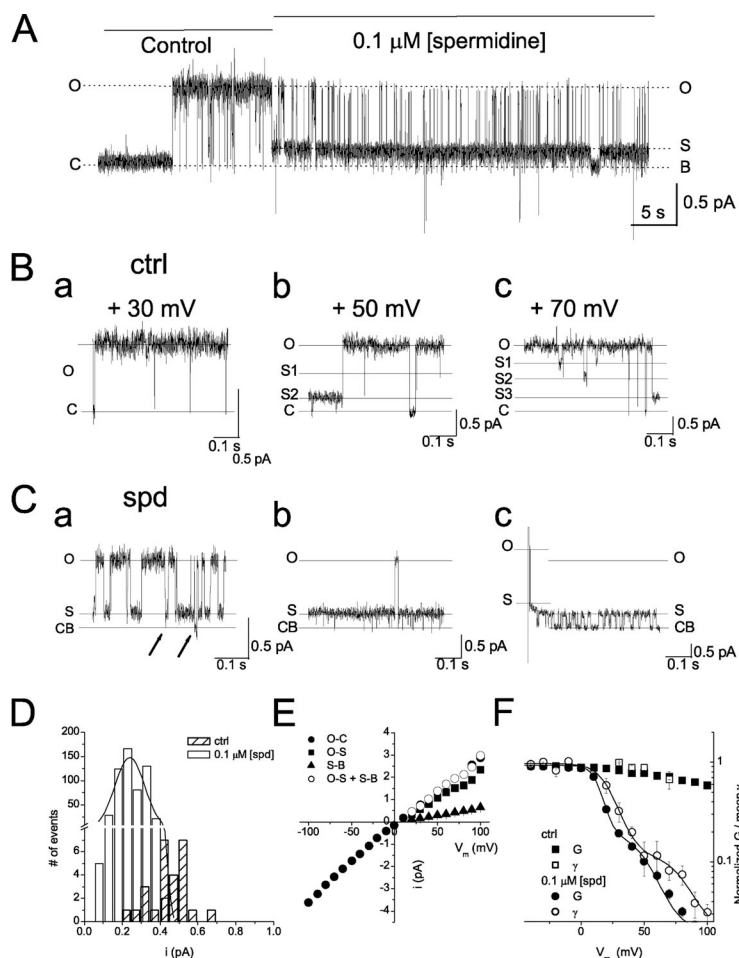

Figure 2. Inhibition of single-channel currents by 0.1 µM [spermidine]$_i$. (A) Single-channel recording obtained at +40 mV in the presence of 150 mM of symmetrical [K$^+$]. (B) Single-channel currents recorded with voltage steps from a holding potential of 0 mV in control at the indicated V_m. Segment of 500-ms recordings are shown. (C) Current traces recorded at 0.1 µM [spermidine]$_i$. (D) Amplitude histograms of substates recorded under control conditions and in the presence of 0.1 µM [spermidine]$_i$ at +40 mV. (E) i–V_m relationships for the fully open state and the O–S and S–B transitions. (F) The voltage dependence of mean single-channel conductance (open symbols) and chord conductance (closed symbols) in the presence of 0.1 µM [spermidine]$_i$. Black lines show fits to Eq. 1, with $A_1 = 0.79$, $A_2 = 0.16$, $V_{h1} = +20.8$ mV, and $V_{h2} = +65.0$ mV, in terms of the mean γ–V_m relationship, and with $A_1 = 0.83$, $A_2 = 0.154$, $V_{h1} = +10.6$ mV, and $V_{h2} = +50.4$ mV, in terms of averaged G–V_m relationships, in the presence of 0.1 µM [spermidine]$_i$. The z_1 and z_2 values were set to 5 and 2.8, respectively. $n = 2$–7. Error bars are not shown when smaller than the symbol.

by arrows in Fig. 2 C, a). The current amplitude between the open state and the substate was 0.60 pA, and that from the substate to the zero-current state was 0.17 pA. At +50 mV (Fig. 2 C, b), the channel stayed mainly in the substate, and the transition between the substate and zero-current state was more frequent than was the case at +30 mV. The channel was seldom in the fully open state, and thus, transitions between the open state and substate were rare (e.g., only one event in 500 ms in Fig. 2 C, b). The difference in current amplitude between the open state and the substate was 1.10 pA, and that from the substate to the zero-current state was 0.31 pA. At $V_m > +50$ mV, the channel transited almost exclusively between the substate and the zero-current state. The fully open state was seldom observed. On rare occasions, the fully open state was noted at the beginning of the depolarization pulse before the channel was subjected to high-affinity block (Fig. 2 C, c). The difference in current amplitude between the open state and the substate was 1.66 pA, and that from the substate to the zero-current state was 0.43 pA.

When the data shown in Figs. 1 and 2 are compared, it is evident that the decrease of the chord conductance of the Kir2.1 channel was mainly the result of high-affinity block at $V_m \leq +30$ mV (Fig. 1 D, b), and the level of single-channel conductance was generally reduced from that of the fully open state to that of the substate with 0.1 µM [spermidine]$_i$ at $V_m = +30$ mV (Fig. 2 C, a). These results indicate that the transition between the fully open state and the substate is attributable to high-affinity block by spermidine. In other words, occupancy of a high-affinity

site by spermidine induces a substate as the mechanism of high-affinity blockade in the Kir2.1 channel. In contrast, once $V_m > +30$ mV, the high-affinity block was near saturated, a further reduction of the chord conductance of the Kir2.1 channel was a result of low-affinity block, and the single-channel recording shows mostly transitions between the substate and the zero-current state. These results suggest that occupancy of the low-affinity site by spermidine induces a completely blocked state in the Kir2.1 channel. The transition directly between the fully open and zero-current states was rarely observed at 0.1 µM [spermidine]$_i$. The O–B transitions happened mostly with a substate in between (240 events out of 269 O to B transitions and 249 events out of 294 B to O transitions at +40 mV). These results indicate that transitions from the substate to the zero-current level are caused mainly by low-affinity spermidine block. Therefore, the zero-current state was considered to be a completely blocked state (B).

Fig. 2 E shows i-V relationships for the fully open state (O–C transition) measured in the absence of spermidine, and for the O–S and S–B transitions measured at 0.1 µM [spermidine]$_i$. The mean single-channel conductance values were 31.8 pS for the O–C transition, 22.9 pS for the O–S transition, and 6.5 pS for the S–B transition. Therefore, the ratio of conductance between O and S states was 3.5:1, similar to that predicted in Scheme 1. The sum of the conductance values for the O–S and S–B transitions was the same as that of the O–C transition, suggesting that the two transitions are two components of a single Kir2.1 channel.
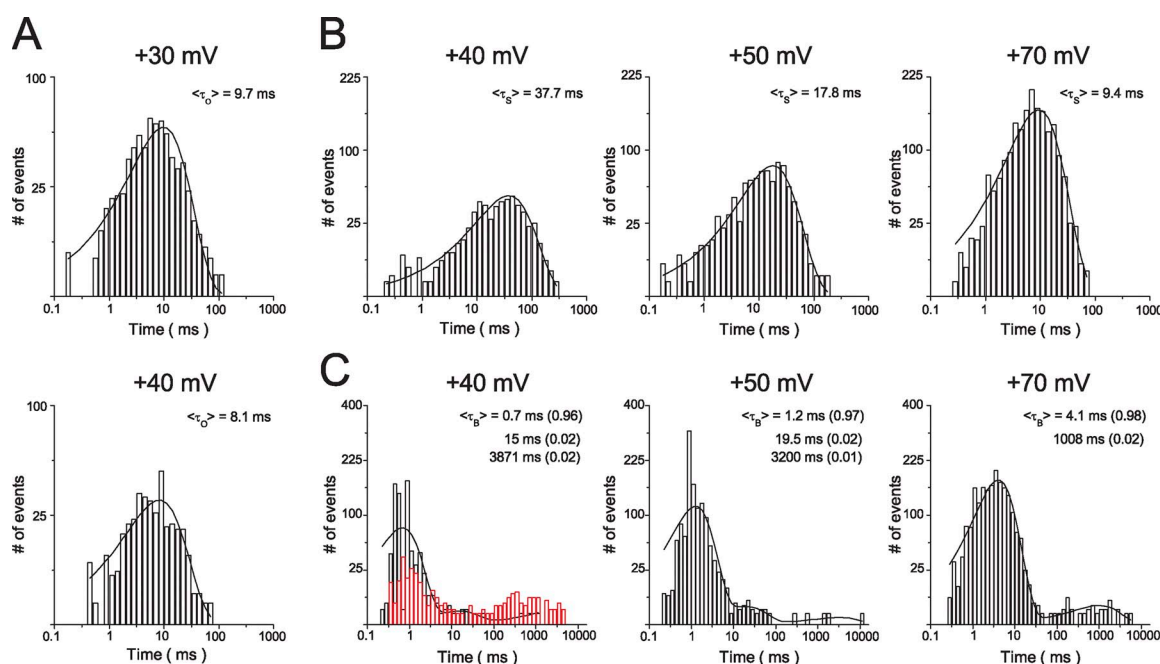

Figure 3. Voltage dependence of the kinetics of spermidine block. (A) Histograms for open times at +30 mV (top) and +40 mV (bottom). (B) Histograms for the substate times at the indicated voltage. (C) Histograms for the blocked times at the indicated voltage. Gray bars are data obtained in the presence of 0.1 µM [spermidine]$_i$, and red bars are those in the control condition.

To compare spermidine block at the single-channel with that at the macroscopic level, we plotted the voltage dependence of mean single-channel conductance (mean current/V_m) and that of normalized chord conductance in the presence of 0.1 µM [spermidine]$_i$. Fig. 2 F shows that the mean γ–V_m and G–V_m relationships were similar. As with the G–V_m relationship, the mean γ–V_m curve at 0.1 µM [spermidine]$_i$ could be described by the sum of two Boltzmann equations (Eq. 1) (Fig. 2 F, black lines), presumably corresponding to high- and low-affinity inhibition by polyamines. In summary, the results show that, at voltages that favor high-affinity block, spermidine reduces single-channel conductance by 78%, similar to the 80% inhibition of chord conductance seen in macroscopic recordings. In other words, the high-affinity spermidine block cannot completely abolish outward Kir2.1 single-channel currents.

Voltage and dose dependence of the transitions between substate and blocked state

Next, we examined the voltage dependence of spermidine block. The kinetics of single-channel currents through the Kir2.1 channel at constant voltages in the presence of 0.1 µM [spermidine]$_i$ was analyzed. Because open events and some blocked events were infrequent, data from different patches were pooled together for histogram construction. Fig. 3 A shows that the open-time histograms were well fitted by single-exponential equations. The mean open time decreased when voltage was more depolarized (9.7 ms at +30 mV and 8.1 ms at +40 mV). The substate time histograms were also well fitted by single-exponential curves (Fig. 3 B). The mean substate time decreased when voltage was more depolarized (37.7 ms at +40 mV, 17.8 ms at +50 mV, and 9.4 ms at +70 mV). Fig. 3 C shows that the blocked-time histograms were fitted by two (+70 mV) or three exponential components (+40 and +50 mV). The dominating ($\geq$96%) short mean blocked times increased from 0.7 to 4.1 ms when voltages were increased from +40 to +70 mV. At all three voltages, rare (~1–2%) but long mean blocked times (>1,000 ms) were observed. At +40 and +50 mV, a medium mean blocked time of 15–20 ms was observed (2%). This component was not obtained from fitting the blocked-time histogram at +70 mV, probably because it is close to the dominating short blocked time (4.1 ms) and is overshadowed. The mean times for the medium and long block could not be accurately determined because of a small number of events. We noted that short, medium, and long blocked (zero-current time) components were also present in the control condition, and that the short blocked (zero-current time) component occurred more frequently in the presence of spermidine than in the control (Fig. 3 C, left, red bars). Because the short closed times had similar values in the absence and presence of spermidine and were spermidine-dose dependent (see Fig. 4), those observed

under control conditions may be the result of the completely blocked state caused by the low-affinity block of residual polyamines. However, if the closed states in nominal polyamine-free solutions are the result of residual block, the high-affinity block ($K_d \sim$ nM) is a more likely candidate than the low-affinity block ($K_d \sim$ µM) (Fig. 1 E). Therefore, we cannot rule out that some or all of the closures are associated with the intrinsic gating
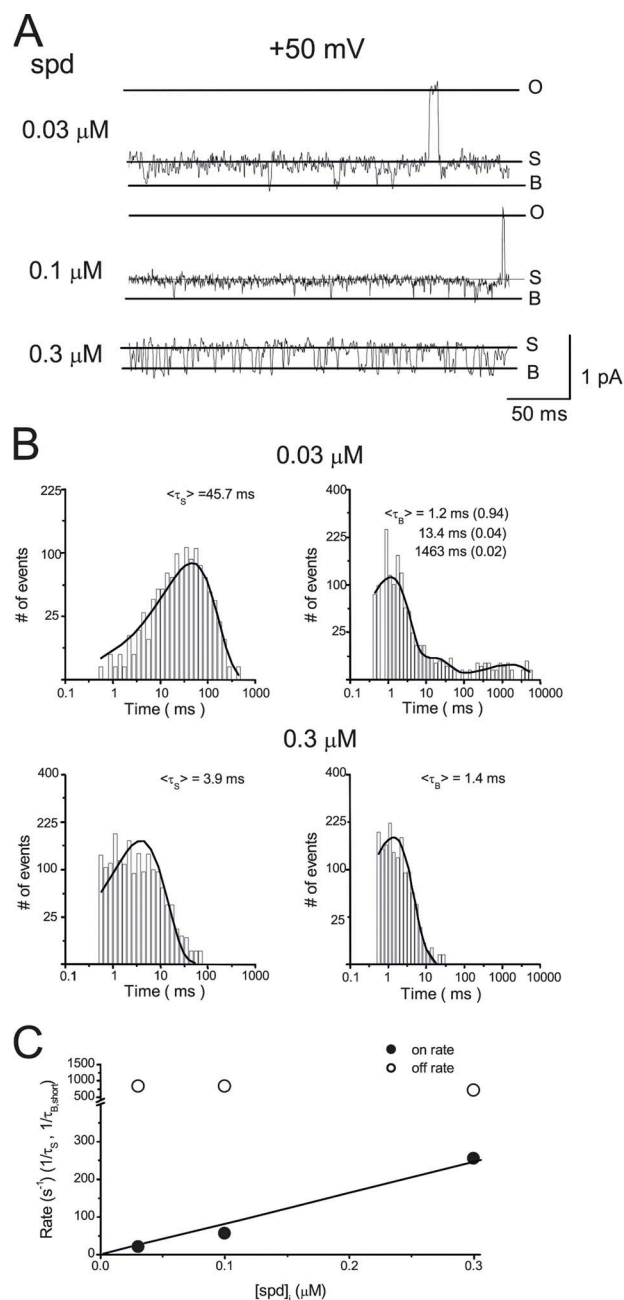

Figure 4. Concentration dependence of the kinetics of spermidine block. (A) Single-channel currents recorded in the presence of 0.03, 0.1, and 0.3 µM [spermidine]$_i$ at +50 mV. (B) Histograms for the substate and blocked times at 0.03 and 0.3 µM [spermidine]$_i$. (C) Dose dependence of association and dissociation rates.

(Matsuda et al., 2003). In the presence of polyamines, the channel is driven into the blocked states (OB$_H$–OB$_{HL}$ reaction) with a blocked time similar to the short component of the intrinsic gating. Alternatively, the zero-current times may be the result of block by other molecules.

Next, we examined the dose-dependent effects of spermidine on the single-channel kinetics. Fig. 4 shows the single-channel recordings (A) and histograms of means substate and blocked times (B) in the presence of 0.03–0.3 μM [spermidine]$_i$ at = +50 mV. When [spermidine]$_i$ was increased, the substate time decreased, whereas the closed times were not affected, suggesting that spermidine acts as an open-channel blocker. Fig. 4 C shows that spermidine association rates ($1/\tau_S$) were linearly dependent on [spermidine]$_i$, but the dissociation rates (estimated as the reverse of the short blocked time) was independent of [spermidine]$_i$. These results support that the transitions between the substate and blocked states are a result of spermidine block.

The substate induced by spermidine was K$^+$ selective and was only observed in membrane patches expressing Kir2.1 channels

To verify that the substate observed in the presence of [spermidine]$_i$ was associated with the Kir2.1 channel, we next determined whether the substate conductance was K$^+$ selective. Fig. 5 shows the single-channel recordings at the indicated voltages in the presence of 20 mM [K$^+$]$_o$ and 150 mM [K$^+$]$_i$, [NH$_4^+$]$_i$, or [Na$^+$]$_i$. In the presence of intracellular K$^+$, outward currents showed substates at voltages ≥ −20 mV (driving forces ≥ +31 mV) in the presence of 0.1 μM [spermidine]$_i$. The substates were similar to those obtained in the presence of 150 mM [K$^+$]$_o$. When intracellular K$^+$ was replaced by NH$_4^+$, inward current was evident at −100 mV, but no current was observed at the voltage range of −20 to +20 mV as a

result of small single-channel conductance (0.4 pA at +50 mV). When intracellular K$^+$ was replaced by Na$^+$, inward current at −100-mV currents appeared flickering, but currents could not be detected at the voltage range of −20 to +20 mV. These results show that the substate is selective for K$^+$.

In addition to manifesting K$^+$ selectivity, the 6.5-pS substate was induced by 0.03–0.3 μM [spermidine]$_i$ in 100 out of 100 patches heterologously expressing Kir2.1 channels but were never observed with spermidine in membrane patches of noninjected oocytes ($n = 10$). Furthermore, the following observations support that the 6.5-pS substate is not attributed to endogenous channels in *Xenopus* oocytes. The most frequently observed endogenous outward currents under our experimental conditions were currents through mechanosensitive channels (Methfessel et al., 1986; Terhag et al., 2010). The percentage of patches (from Kir2.1 cRNA-injected oocytes) expressing the mechanosensitive channel was ∼30–50%. The percentage of patches expressing other non-Kir2.1 channels was <1%. Fig. 6 shows single-channel currents through the mechanosensitive endogenous channel. The single-channel conductance for K$^+$ was 31.9 ± 1 pS ($n = 2$) at 0 mV, similar to that of the Kir2.1 channel (29.2 ± 1.2 pS; $n = 3$). In addition, the open probability was higher at a more depolarized voltage, as reported previously (Silberberg and Magleby, 1997), and it was larger than that of the Kir2.1 channel. Therefore, when this channel was present, outward Kir2.1 channel could not be studied and the patch was discarded. Fig. 6 shows that the mechanosensitive channel was not selective to cations; intracellular K$^+$, NH$_4^+$, and Na$^+$ were all permeable through the channel (Yang and Sachs, 1990). Furthermore, in the presence of 0.1 μM spermidine, substate was not observed. These results suggest that the substate associated with spermidine block is
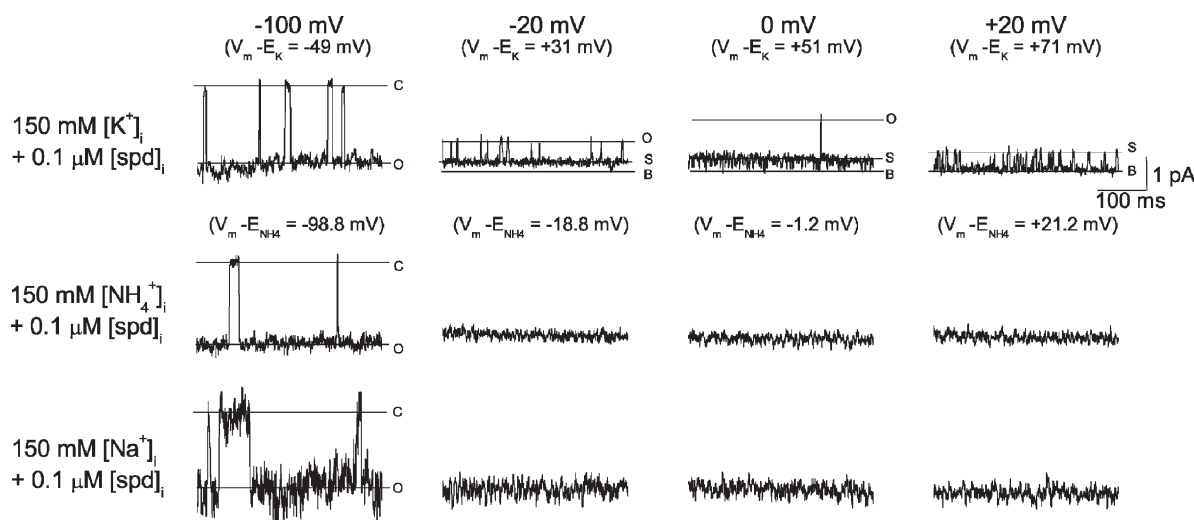

Figure 5. Substate induced by 0.1 μM [spermidine]$_i$ was selective for K ions. Single-channel currents recorded in the presence of 20 mM [K$^+$]$_o$ and the indicated intracellular ions. Similar results were found in six other patches.
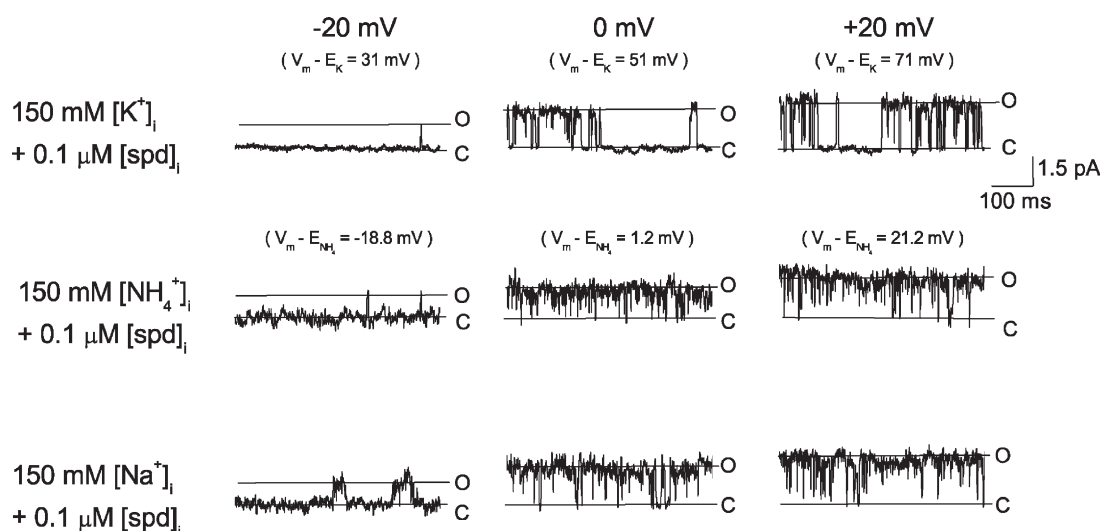
Figure 6. The most frequent observed endogenous channels were not cation selective. Single-channel recordings in the presence of 20 mM $[K^+]_o$ and the indicated intracellular solution. Similar observations were made in five other patches.

not contributed by the endogenous mechanosensitive channel. Furthermore, the voltages, where the substate associated with spermidine appeared, shifted with E_K but not E_{Cl} when $[KCl]_o$ was changed, suggesting that

the substate is not associated with endogenous Cl^- channels. These results collectively support the conclusion that the substate induced by spermidine is attributed to K^+ going through single Kir2.1 channels.
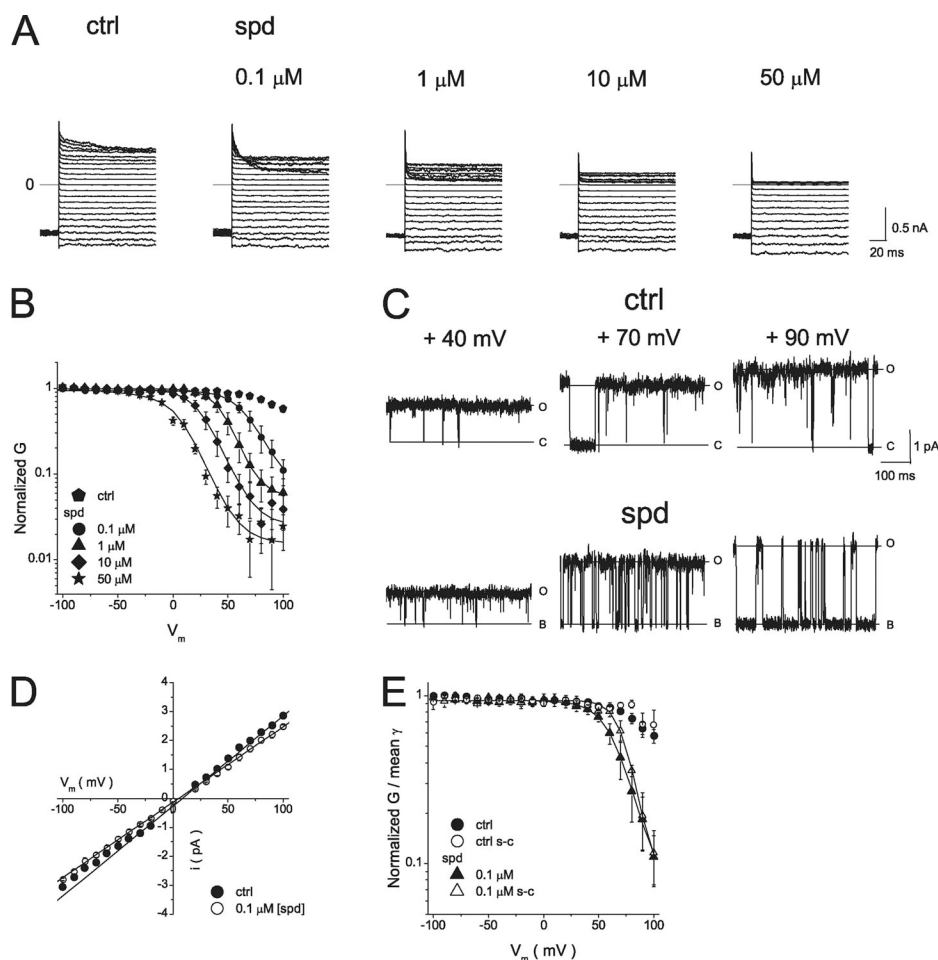

Figure 7. Inhibition of D172N currents by intracellular spermidine. (A) Currents in D172N mutants were recorded using inside-out giant patches under control conditions and in the presence of the indicated concentrations of spermidine (spd). Currents were recorded using the protocol described in Fig. 1 A. (B) Normalized $G–V_m$ relationships shown on a semilogarithmic scale. Black lines show fits to a single Boltzmann equation, with z = 2.0/V_h = +66 mV (0.1 µM $[spermidine]_i$), z=2.6/V_h=+44.8 mV (1 µM $[spermidine]_i$), and z = 2.3/V_h = +25.4 mV (10 µM $[spermidine]_i$). (C) Single-channel currents recorded under control conditions at the indicated V_m values. (D) i–V_m relationships for the conductive states were ohmic, both under control conditions (O–C) and at 0.1 µM $[spermidine]_i$ (O–B). n = 3. Error bars are not shown when smaller than the symbols. (E) Mean $\gamma–V_m$ and normalized $G–V_m$ relationships under control conditions and in the presence of 0.1 µM $[spermidine]_i$. The black line shows the single Boltzmann relationship fitted to single-channel data, with z = 2.9/V_h = +74.3 mV.

Spermidine did not induce a substate in a D172N mutant lacking the high-affinity binding site

If the substate introduced by spermidine is attributable to high-affinity channel blockade, the substate should not be observed in the D172N mutant, in which the high-affinity binding site is effectively destroyed (Stanfield et al., 1994; Wible et al., 1994; Yang et al., 1995a; Ishihara and Yan, 2007). To confirm that the D172N mutant was sensitive only to low-affinity block, we explored the effects of spermidine on D172N currents. Fig. 7 A shows currents through the D172N mutant recorded in the absence (control) and presence of the indicated [spermidine]$_i$. Fig. 7 B shows normalized G–V$_m$ relationships, which could be well described by a single Boltzmann equation (black lines) with equivalent charges (z values) of 2.0 (0.1 µM [spermidine]$_i$), 2.6 (1 µM [spermidine]$_i$), and 2.3 (10 µM [spermidine]$_i$). The G–V$_m$ relationship obtained in the presence of 50 µM [spermidine]$_i$ displayed a shallow component in the negative voltage range probably because of a surface charge effect (Xie et al., 2002), and was thus fitted by a double Boltzmann equation with $z_1 = 0.3/V_{h1} = −22.4$ mV, and $z_2 = 3.0/V_{h2} = +8.9$ mV. These values of the equivalent spermidine block charges were similar to those associated with low-affinity block described above for wild-type channels and therefore support the notion that the D172N mutant is sensitive to low- but not high-affinity block. Next, we determined whether spermidine block could induce a substate in the D172N mutant. Fig. 7 C shows the single-channel currents recorded at +40, +70, and +90 mV under control conditions, and in the presence of 0.1 µM [spermidine]$_i$. At +40 mV, the channel remained principally in the fully open state, both under control conditions and at 0.1 µM [spermidine]$_i$. At +70 and +90 mV, where low-affinity block was strong, the channel transited between the fully open and zero-current states more frequently in the presence of 0.1 µM [spermidine]$_i$ than under control conditions. The mean currents were smaller at 0.1 µM [spermidine]$_i$ than under control condition (see Fig. 7 E), suggesting that low-affinity block was evident, despite the low dose. However, 0.1 µM [spermidine]$_i$ did not induce substate formation in the D172N mutant. These results suggest that the wild-type channel substate induced by spermidine is not associated with low-affinity block. Fig. 7 D shows the voltage dependence of the single-channel current in the fully open state in both the absence and presence of 0.1 µM [spermidine]$_i$. The single-channel conductance for the O–C transition (control, $27.9 ± 3.8$ pS; $n = 3$) did not differ significantly ($P = 0.42$) from that of the O–B transition (0.1 µM [spermidine]$_i$, $25.9 ± 1.5$ pS; $n = 3$). To compare the spermidine block at the single-channel level with that at the macroscopic level, we compared the voltage dependence of mean single-channel and chord conductance. Fig. 7 E shows that the mean γ–V$_m$ relationship obtained

in the presence of 0.1 µM [spermidine]$_i$ in the D172N mutant was well fitted by a single Boltzmann equation with an equivalent moving charge of 2.4. This charge was similar to that seen upon low-affinity block of the
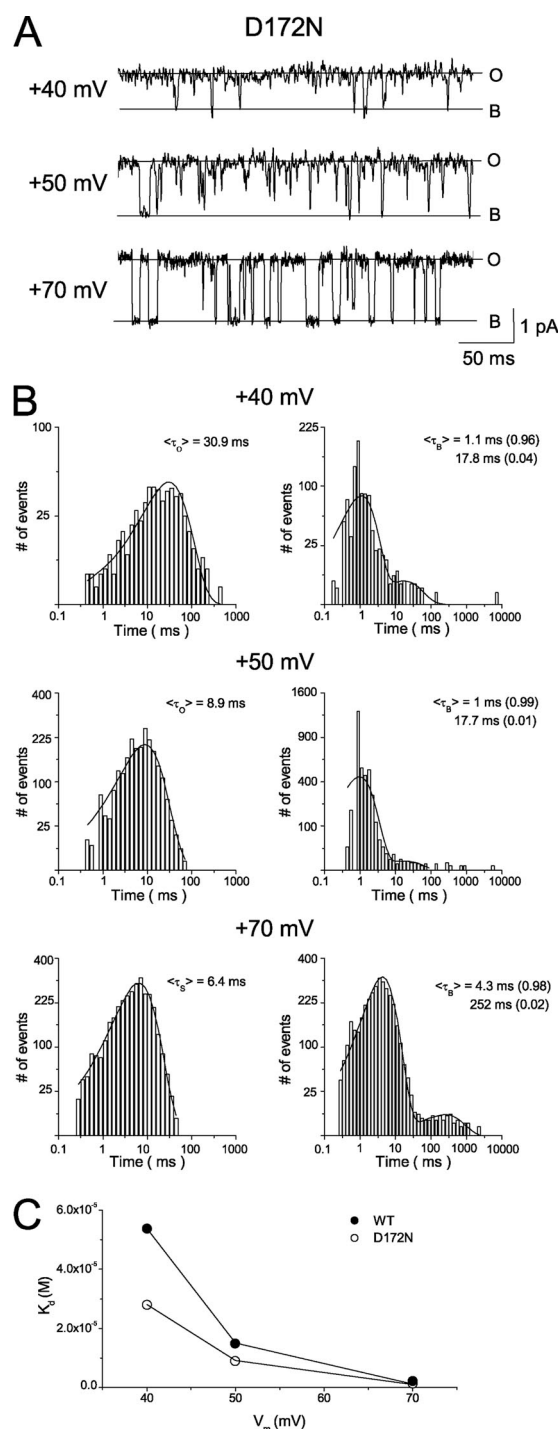

Figure 8. Voltage dependence of spermidine block in the D172N mutant. (A) Single-channel currents recorded in the presence of 0.1 µM [spermidine]$_i$ at +40, +50, and +70 mV. (B) Histograms for the substate and blocked times. (C) Voltage dependence of dissociation constants for the wild-type Kir2.1 (closed symbols) and the D172N mutant (open symbols).

wild-type channel (z = 2.8; Fig. 1) and that obtained by study of macroscopic currents in D172N mutants (z = 2.0; Fig. 7 B). These results support the notion that the D172N mutant is susceptible only to low-affinity block and that the substate induced by spermidine is attributable to high-affinity block in the wild-type channel.

Transition between the substate and the blocked state was attributable to low-affinity block

Because the low-affinity polyamine block in the wild-type is similar to the polyamine block in the D172N mutant, the kinetics of the S–B transition should be similar to the O–B transition in the D172N mutant in the presence of spermidine if the S–B transition represents a low-affinity block of the wild-type Kir2.1 channel. Fig. 8 A shows the single-channel currents recorded at +40, +50, and +70 mV in the presence of 0.1 µM [spermidine]$_i$. Fig. 8 B shows that the open-time histograms were well fitted by single-exponential curves. The mean open times were 30.9 ms at +40 mV, 8.9 ms at +50 mV, and 6.4 ms at +70 mV. These values were slightly smaller than those obtained in the wild-type Kir2.1 channel probably because the D172N mutation affects the kinetics of low-affinity block. For example, the blocker's on-rate for the low-affinity binding site may be decreased if the pore has already been occupied by a positively charged blocker at the high-affinity site (D172) in the wild-type Kir2.1 channel. Fig. 8 B shows that the blocked-time histograms were fitted by two exponential components. Similar to the wild-type channel, the dominating (96–99%) mean blocked times increased from 1 to 4.3 ms when voltages were increased from +40 to +70 mV. An infrequent (1–4%) medium blocked time of around 18 ms was observed at +40 and +50 mV, and some rare but long blocked events (>100 ms) were observed at all three voltages in the D172N mutant. The long blocked component may contribute to the pedestal current, which is sensitive to polyamine block in a voltage-independent way. Because the long blocked time was shorter and the percentage of this component was smaller in the D172N mutant than in the wild-type Kir2.1 channel, the voltage-independent component was more obvious in the G–V$_m$ relationship in the D172N mutant (Fig. 7 B) than that in the wild type (Fig. 1 C, b). It is noted that this component is not involved in the substate induced by spermidine block and contributes only 2% in the wild-type channel. To further compare the S–B transitions in the wild-type Kir2.1 channel with the O–B transitions in the D172N mutant, we estimated the equivalent valence from the voltage dependence of spermidine dissociation constants calculated from the mean substate/open time and blocked time. Fig. 8 C shows that the K$_d$–V$_m$ relationships were fitted by a Boltzmann equation with z = 2.9 in the wild-type Kir2.1 channel and z = 2.6 in the D172N mutant. These values were similar to each other and to the equivalent charges estimated from G–V$_m$

relationships, suggesting that spermidine block in the D172N mutant is comparable to the low-affinity block in the wild-type Kir2.1 channel.

Next, we compared the dose dependence of spermidine block in the D172N mutant to that of low-affinity block in the wild-type channel. Fig. 9 shows the single-channel recordings (A) and histograms of means substate and blocked times (B) in the presence of 0.03–0.3 µM [spermidine]$_i$ at = +50 mV. Fig. 9 C shows that the association rates (1/τ$_O$) were linearly dependent on [spermine]$_i$, whereas the dissociation rates were independent of
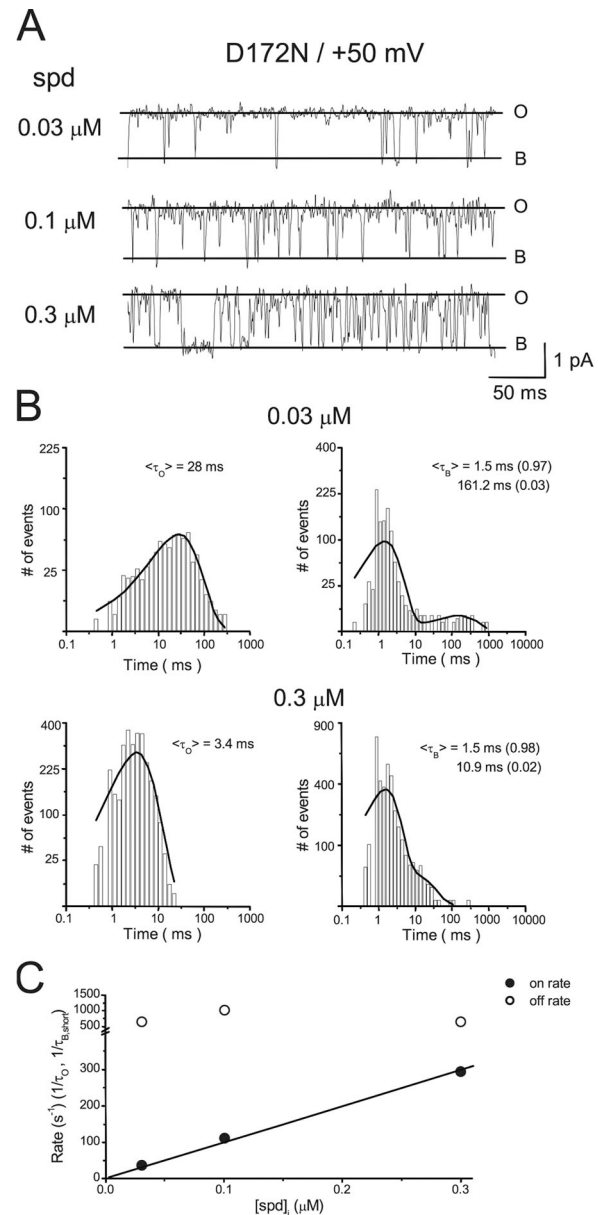

Figure 9. Concentration dependence of the kinetics of spermidine block in the D172N mutant. (A) Single-channel currents recorded in the presence of 0.03, 0.1, and 0.3 µM [spermidine]$_i$ at +50 mV in the D172N mutant. (B) Histograms for the substate and blocked times. (C) Dose dependence of association and dissociation rates.

[spermidine]$_i$ in the D172N mutant. These results are similar to those observed in the wild-type channel (Fig. 4 C). In summary, these collective results support the ideas that the substate is generated by an incomplete high-affinity block of the single Kir2.1 channel, and that the S–B transition is attributable to low-affinity block by spermidine.

DISCUSSION

K ions permeate through the Kir2.1 channel during high-affinity polyamine block

Outward currents through inward rectifier K$^+$ channels are important in regulating the electrical properties of cells, despite the small amplitude thereof, owing to inward rectification. Both high- and low-affinity polyamine blocks have been identified and characterized in the Kir2.1 channel (Stanfield et al., 1994; Wible et al., 1994; Yang et al., 1995a; Kubo and Murata, 2001; Ishihara and Yan, 2007). However, the relative contribution of the high- and low-affinity blocks to the emergence of outward Kir2.1 currents is not well understood. Under physiological conditions ($\sim$1–10 μM [spermine]$_i$), high-affinity block should be saturated, and thus a component of the Kir2.1 channel must be insensitive to high-affinity block in order for outward currents to occur (Ishihara and Ehara, 2004; Ishihara and Yan, 2007). By using a low concentration of spermidine, instead of spermine, we were able to investigate the details of high- and low-affinity block at the single-channel level. We show that occupancy of a high-affinity site by spermidine induces a substate as the mechanism of high-affinity block, and occupancy of the low-affinity site by spermidine induces a completely blocked state of the Kir2.1 channel. At voltages where the high-affinity block predominates, spermidine induces a Kir2.1 channel substate, the conductance of which is 6.5 pS. Similar substates induced by 10 nM spermidine have been observed previously (Ficker et al., 1994). At voltages where the high-affinity block is saturated and at the same time the low-affinity block is favored, the channel transits between the substate and the zero-current state, suggesting that the zero-current state represents the low-affinity block state. Although we explained our experimental results with two distinct polyamine-binding sites, an alternative explanation is that the substate represents spermidine binding in the water cavity, but the fully blocked state is caused by the same spermidine, with its leading amine inserted in the selectivity filter as suggested by previous studies (John et al., 2004; Kurata et al., 2004, 2006). This latter scheme will predict that the equivalent moving charge, z, for spermidine block in the D172N mutant is closed to $z_1 + z_2$ estimated in the wild-type channel. On the contrary, we found that the z value of the D172N mutant is the same as z_2 (equivalent moving charge for low-affinity block) rather than as $z + z_2$ in the

wild-type channel (Ishihara and Yan, 2007). In addition, the dwell times for S–B transitions in the wild-type Kir2.1 channel are very similar, if not identical, to those of the O–B transitions in the D172N mutant, further supporting the idea that the S–B transition is attributable to low-affinity block by spermidine, as the high-affinity site for polyamines block was effectively eliminated by the D172N mutation (Ishihara and Yan, 2007). Thus, our results are consistent with previous studies suggesting that the Kir2.1 channel can accommodate more than one blocking molecule (Yang et al., 1995b; Guo and Lu, 2000). Although we observed that spermidine induced substates in all 100 patches studied and we had never found two populations of Kir channels sensitive to only high- or low-affinity block, respectively, we could not completely exclude the possibility that a two-population hypothesis may also explain the incomplete high-affinity block under certain experimental conditions.

Fig. 10 shows a schematic illustration of how high- and low-affinity blocks regulate outward Kir2.1 currents to cause inward rectification and to form a hump-shape I–V$_m$ relationship. During weak depolarization where the slope of the I-V relationship is positive (Fig. 10 A, blue shaded area), the probability of high-affinity block is very high and that of low-affinity block low. When a polyamine enters the Kir2.1 channel, the molecule binds to the high-affinity site involving D172 and induces formation of a substate (Fig. 10 B, S state). The channel thus usually stays in either the fully open state or the substate. In other words, the positive slope of the hump-shape I–V$_m$ relationship is attributable to K$^+$ conduction through both the fully open state and the substate. This has been discussed previously in terms of polyamine block of the Kir2.1 channel in state I and relief thereof (Ishihara and Ehara, 2004). During strong depolarization (corresponding to the negatively sloped region of the I–V$_m$ relationship; Fig. 10 A, purple-shaded area), the high-affinity block becomes saturated and the main conducting state is the substate. In addition, the probability of low-affinity block increases (S–B transitions become more frequent) as the voltage becomes increasingly depolarized. Therefore, the outward Kir2.1 current decreases as depolarization is stronger, and the slope of the I-V relationship becomes negative. This has been described as polyamine block of the Kir2.1 channel in state II (Ishihara and Ehara, 2004). Because the O–B transitions happened mostly with a substate (dwell time, >0.1 ms) in between (240 events out of 269 O to B transitions and 249 events out of 294 B to O transitions at +40 mV), we would note that low-affinity block occurs mostly, if not exclusively, as a transition from the substate rather from the open state, and the O–S–B transitions thus occur in that sequence. In addition, C–O transitions are rare because of saturation of the high-affinity block that drives the channel into the substate. According to the O–S–B scheme, the normalized steady-state G–V$_m$
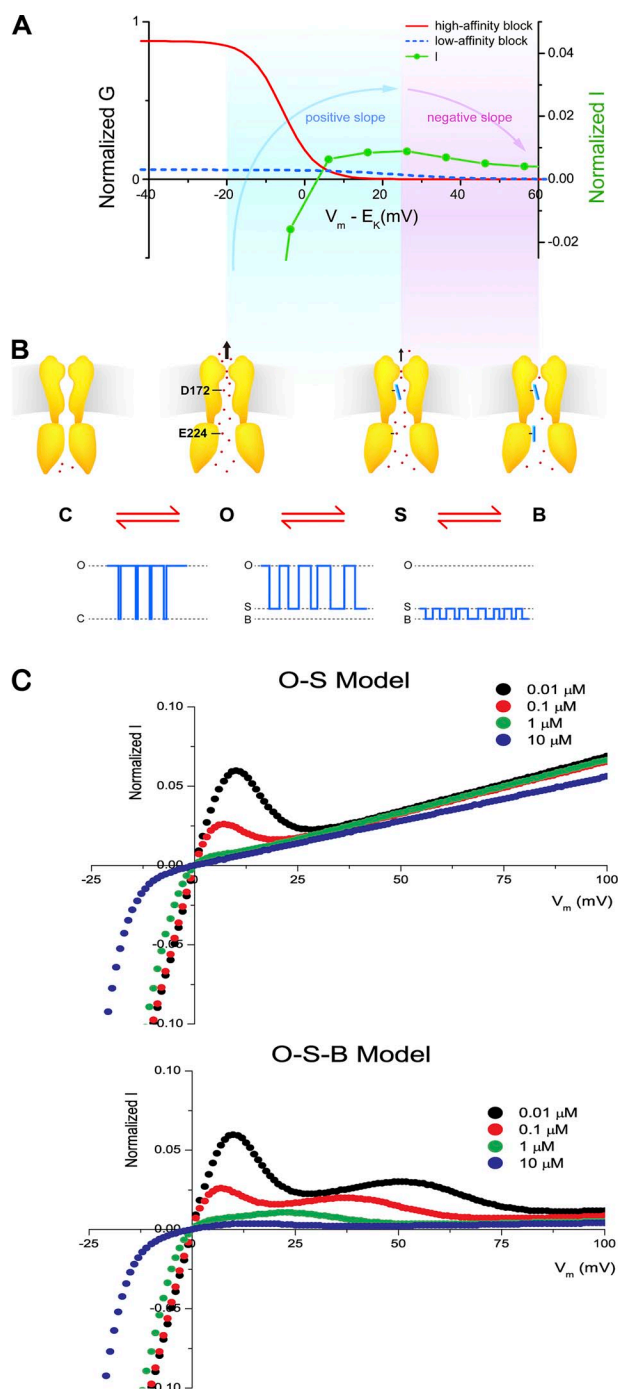
Figure 10. The O–S–B Model for the regulation of outward Kir2.1 currents by high-affinity and low-affinity polyamine blocks. (A) The dependence of chord conductance and currents on driving force ($V_m–E_K$). Red line indicates the conductance sensitive to high-affinity block, and blue dash denotes low-affinity block of conductance. The blue-shaded area indicates the voltage range where the slope of I–V_m relationship is positive, and the purple-shaded area indicates the voltage range with negative slope. (B) Cartoons of the channels in C, O, S, and B states and the corresponding single-channel currents. Red dots indicate K ions. (C) Steady-state I–V_m relationships in the presence of only high-affinity block by spermine at the indicated concentrations are shown in the top panel. Currents = $G/G_{max} \times V_m$, and G/G_{max} values were calculated from Eq. S6, with A_1, A_2, z_1, and V_{h1} listed in

relationship can be expressed by Eq. S3 and, under our experimental conditions, can be approximated by the sum of two Boltzmann relationships (supplemental text). Fig. S1 shows that the normalized G–V_m relationships can be fitted by Eq. S3.

The permeability of K ions during high-affinity polyamine block depends on the blocker used. Single-channel block is 78% and chord-conductance block is 80% in the high-affinity spermidine mode, whereas chord conductance block in the high-affinity spermine situation is 93%. Similar macroscopic data have been obtained previously (Ishihara and Ehara, 2004). One reason why incomplete single-channel inhibition by high-affinity polyamine block has not been described previously is that spermine instead of spermidine was usually chosen as the experimental blocker. Because the substate induced by spermine (~1.9 pS at 150 mM of symmetrical $[K^+]$) does not differ greatly from the zero-current state, the fact that block is incomplete could not be easily noted. Furthermore, because the substate is not obvious, analysis of blocked times (to obtain the dissociation rate constant) upon high-affinity block may have been confounded by the presence of some low-affinity block if membrane voltage is strong depolarized. However, the analysis of open times (thus reflecting the association rate under high-affinity spermine block conditions) should remain valid.

Subconducting states in Kir2.1 channels

Various levels of subconducting states have been described for inward currents through Kir2.1 channels. It has been shown that 100 µM and 1 mM [spermine]$_i$ induce substates for inward K^+ conductance in the Kir2.1 channel by a surface charge screening effect involving E224 and E299 located in the cytoplasmic pore (Xie et al., 2002). The substate induced by 0.1 µM [spermidine]$_i$ for outward K^+ conductance shown in this study is probably not attributed to the same mechanism for the following reasons. First, the spermidine-induced substate is not observed in the D172N mutant where the E224 and E299 sites are intact. Second, the dissociation constant for the surface charge–screening effect is around 1 µM for spermine (Xie et al., 2002), and this value should be higher for spermidine with a lower affinity. Therefore, the low [spermidine]$_i$ (0.1 µM) used in this study should have limited surface charge–screening capability.

Another type of substate in the Kir2.1 channel is PIP_2 dependent. It has been shown that PIP_2 molecules interact with Kir2.1 subunits at the cytoplasmic domain,

Table S2. Steady-state I–V_m relationships in the presence of both high- and low-affinity block by spermine are shown in the bottom panel. G/G_{max} values were calculated from Eq. S3, with A, A_2, z_1, z_2, V_{h1}, and V_{h2} listed in Table S2.

and the interaction stabilizes the channel in the fully open state (Xie et al., 2008). Inhibition of this interaction induces substates of various levels before channel rundown. It has been shown that intracellular polyamines stabilize the interaction of PIP_2 and the Kir2.1 channel (Xie et al., 2005). Therefore, polyamines should prevent substates of various levels associated with PIP_2 depletion from occurring. The substate induced by intracellular spermidine is thus distinct from the PIP_2-dependent ones.

High-affinity binding site for polyamines

Ions are generally thought to move through K^+ channels in single file. However, when the channel is in the substate, K^+ ions can apparently pass by spermidine bound in the water cavity and exit the channel via the selectivity filter, suggesting that the water cavity is sufficiently large to allow non–single file movement. Indeed, it has been shown previously that the water cavity can accommodate three 10-Å and one 3.6-Å positively charged molecules, suggesting that the region would allow simultaneous occupancy by three partially hydrated Mg^{2+} ions or three vertically aligned polyamines (Lu et al., 1999). In addition, the crystal structure of a Kir2.2 channel in an open configuration has been resolved (Hansen et al., 2011). The diameter of the space formed by four D173 (equivalent to D172 in Kir2.1) is 13 Å, large enough for K^+ conductance when a polyamine blocks at this site. These previous studies and the present work support the idea that ion permeation through the water cavity may not occur in single file, as traditionally proposed for the Kir channels (Hille and Schwarz, 1978). Exactly how spermidine binds to the high-affinity site in the water cavity and whether other residues, besides D172, interact with spermidine such that K^+ ions can bypass this interaction require further investigation.

It is noted that the above-mentioned non–single file movement occurs at the large water cavity and may not be applied to a constricted area. For example, it has been shown that four symmetrical cytoplasmic loops consisting of Gly-Phe-Asp-Ser-Gly residues constrict the cytoplasmic pore to <10 Å (Xu et al., 2009). These loops may encircle a polyamine entering the pore and prevent K^+ ions from bypassing the area and then leaking into the intracellular side (Xu et al., 2009).

Physiological implications

It is noted that, under physiological conditions, Kir2.1 channel block by spermine is probably dominant, in the sense that spermine is more important than other intracellular blockers (Ishihara and Ehara, 2004). The I–V_m relationships obtained using native cells are similar to those recorded with 5–10 µM [spermine]$_i$ in HEK293 cells (Ishihara and Ehara, 2004) and with ~0.1–1 µM [spermine]$_i$ in oocytes (Fig. 1). To evaluate whether outward K^+ currents can go through the substate at physiological concentrations of spermine, I–V_m relationships in the presence of only high-affinity block were simulated using the O–S model (see supplemental text). Fig. 10 C shows the I–V_m relationships predicted by Eq. S5 in the presence of only high-affinity block by 0.01–10 µM [spermine]$_i$ (top). The I–V_m relationships were ohmic, except for a narrow hump at the voltage range of 0 to +20 mV at 0.01 and 0.1 µM [spermine]$_i$. However, in the presence of both high- and low-affinity blocks, the I–V_m relationships predicted by the O–S–B model (Eq. S3) showed inward rectification at 0.01–10 µM [spermine]$_i$ (Fig. 10 C, bottom). The simulations suggest that fair amounts of K^+ ions can efflux through the Kir2.1 channel, presumably through the substate, in the presence of saturated high-affinity block, and that the low-affinity block determines the amplitude of outward currents under physiological conditions (Ishihara and Ehara, 2004). It is thus important to understand the process of low-affinity block in detail. Previous studies have shown that low-affinity block involves binding of polyamines to cytoplasmic pores (Yang et al., 1995a; Kubo and Murata, 2001). It remains unclear how polyamines binding to the cytoplasmic pores (low-affinity block) outside of the electrical field (Tao et al., 2009) can cause voltage-dependent inhibition of outward currents. Some studies suggest that the interaction of polyamine with E224 and E299 is coupled to the high-affinity block in the water cavity (Guo and Lu, 2003; Guo et al., 2003). It is also possible that a polyamine interacting with the cytoplasmic pore may eventually completely block the pore at or near site D172, with low affinity after the initial polyamine partially plugs the pore at D172 with high affinity (Kubo and Murata, 2001; Xie et al., 2003). This mechanism could readily explain the voltage dependence of the low-affinity block. However, it might not predict that the on-rate for the block is proportional to the blocker concentration, as it would not involve movement of the blocker into the pore from the bulk solution. In addition, the model would predict that the low-affinity block is reduced by the D172N mutation. Alternatively, some studies suggest that polyamines bound at the cytoplasmic pore may decrease K^+ efflux via an electrostatic effect (Lee et al., 1999; Yeh et al., 2005; Fujiwara and Kubo, 2006; Chang et al., 2007). It seems counterintuitive that the low-affinity inhibition at the more superficial and wider cytoplasmic is more "complete" than the high-affinity block deep within the pore. Nevertheless, it is not physically impossible. For example, polyamines bound at the cytoplasmic pore may decrease K^+ occupancy in the selectivity, dramatically decrease K^+–K^+ interaction, and thus reduce K^+ conductance as hypothesized previously (Yeh et al., 2005). The distinct and separable characteristics of high- and low-affinity block at the single-channel level may be a useful vehicle for further characterization of low-affinity block in Kir channels.

Conclusions

Outward Kir2.1 currents are important in controlling the electrical properties of excitable cells. Under physiological conditions, outward currents can still go through Kir2.1 channels when high-affinity polyamine block is saturated. We have shown at the single-channel level that the incompleteness of high-affinity block is attributable to K^+ ions permeating through Kir2.1 channels. Thus, the amplitudes of outward Kir2.1 currents are determined by voltage-dependent inhibition, via low-affinity polyamine block, of outward currents that persist even in the presence of a saturated high-affinity block. This study provides a more detailed insight into the mechanism underlying the emergence of outward currents regulated by inward rectification.

REFERENCES

Chang, H.K., S.H. Yeh, and R.C. Shieh. 2005. A ring of negative charges in the intracellular vestibule of Kir2.1 channel modulates K^+ permeation. *Biophys. J.* 88:243–254. http://dx.doi.org/10.1529/biophysj.104.052217

Chang, H.K., S.H. Yeh, and R.C. Shieh. 2007. Charges in the cytoplasmic pore control intrinsic inward rectification and single-channel properties in Kir1.1 and Kir2.1 channels. *J. Membr. Biol.* 215:181–193. http://dx.doi.org/10.1007/s00232-007-9017-0

Constanti, A., and M. Galvan. 1983. Fast inward-rectifying current accounts for anomalous rectification in olfactory cortex neurones. *J. Physiol.* 335:153–178.

Day, M., D.B. Carr, S. Ulrich, E. Ilijic, T. Tkatch, and D.J. Surmeier. 2005. Dendritic excitability of mouse frontal cortex pyramidal neurons is shaped by the interaction among HCN, Kir2, and Kleak channels. *J. Neurosci.* 25:8776–8787. http://dx.doi.org/10.1523/JNEUROSCI.2650-05.2005

Ficker, E., M. Taglialatela, B.A. Wible, C.M. Henley, and A.M. Brown. 1994. Spermine and spermidine as gating molecules for inward rectifier K^+ channels. *Science*. 266:1068–1072. http://dx.doi.org/10.1126/science.7973666

Fujiwara, Y., and Y. Kubo. 2006. Functional roles of charged amino acid residues on the wall of the cytoplasmic pore of Kir2.1. *J. Gen. Physiol.* 127:401–419. http://dx.doi.org/10.1085/jgp.200509434

Guo, D., and Z. Lu. 2000. Mechanism of IRK1 channel block by intracellular polyamines. *J. Gen. Physiol.* 115:799–814. http://dx.doi.org/10.1085/jgp.115.6.799

Guo, D., and Z. Lu. 2003. Interaction mechanisms between polyamines and IRK1 inward rectifier K^+ channels. *J. Gen. Physiol.* 122:485–500. http://dx.doi.org/10.1085/jgp.200308890

Guo, D., Y. Ramu, A.M. Klem, and Z. Lu. 2003. Mechanism of rectification in inward-rectifier K^+ channels. *J. Gen. Physiol.* 121:261–275. http://dx.doi.org/10.1085/jgp.200208771

Hamill, O.P., A. Marty, E. Neher, B. Sakmann, and F.J. Sigworth. 1981. Improved patch-clamp techniques for high-resolution current recording from cells and cell-free membrane patches. *Pflugers Arch.* 391:85–100. http://dx.doi.org/10.1007/BF00656997

Hansen, S.B., X. Tao, and R. MacKinnon. 2011. Structural basis of PIP2 activation of the classical inward rectifier K^+ channel Kir2.2. *Nature*. 477:495–498. http://dx.doi.org/10.1038/nature10370

Hilgemann, D.W. 1995. The giant membrane patch. *In* Single-Channel Recording. B. Sakmann and E. Neher, editors. Plenum Press, New York. 307–328.

Hille, B., and W. Schwarz. 1978. Potassium channels as multi-ion single-file pores. *J. Gen. Physiol.* 72:409–442. http://dx.doi.org/10.1085/jgp.72.4.409

Hume, J.R., and A. Uehara. 1985. Ionic basis of the different action potential configurations of single guinea-pig atrial and ventricular myocytes. *J. Physiol.* 368:525–544.

Ishihara, K., and T. Ehara. 2004. Two modes of polyamine block regulating the cardiac inward rectifier K^+ current IK1 as revealed by a study of the Kir2.1 channel expressed in a human cell line. *J. Physiol.* 556:61–78. http://dx.doi.org/10.1113/jphysiol.2003.055434

Ishihara, K., and D.H. Yan. 2007. Low-affinity spermine block mediating outward currents through Kir2.1 and Kir2.2 inward rectifier potassium channels. *J. Physiol.* 583:891–908. http://dx.doi.org/10.1113/jphysiol.2007.136028

John, S.A., L.H. Xie, and J.N. Weiss. 2004. Mechanism of inward rectification in Kir channels. *J. Gen. Physiol.* 123:623–625. http://dx.doi.org/10.1085/jgp.200409017

Kubo, Y., and Y. Murata. 2001. Control of rectification and permeation by two distinct sites after the second transmembrane region in Kir2.1 K^+ channel. *J. Physiol.* 531:645–660. http://dx.doi.org/10.1111/j.1469-7793.2001.0645h.x

Kubo, Y., T.J. Baldwin, Y.N. Jan, and L.Y. Jan. 1993. Primary structure and functional expression of a mouse inward rectifier potassium channel. *Nature*. 362:127–133. http://dx.doi.org/10.1038/362127a0

Kurata, H.T., L.R. Phillips, T. Rose, G. Loussouarn, S. Herlitze, H. Fritzenschaft, D. Enkvetchakul, C.G. Nichols, and T. Baukrowitz. 2004. Molecular basis of inward rectification: polyamine interaction sites located by combined channel and ligand mutagenesis. *J. Gen. Physiol.* 124:541–554. http://dx.doi.org/10.1085/jgp.200409159

Kurata, H.T., L.J. Marton, and C.G. Nichols. 2006. The polyamine binding site in inward rectifier K^+ channels. *J. Gen. Physiol.* 127:467–480. http://dx.doi.org/10.1085/jgp.200509467

Lee, J.K., S.A. John, and J.N. Weiss. 1999. Novel gating mechanism of polyamine block in the strong inward rectifier K channel Kir2.1. *J. Gen. Physiol.* 113:555–564. http://dx.doi.org/10.1085/jgp.113.4.555

Lopatin, A.N., E.N. Makhina, and C.G. Nichols. 1994. Potassium channel block by cytoplasmic polyamines as the mechanism of intrinsic rectification. *Nature*. 372:366–369. http://dx.doi.org/10.1038/372366a0

Lu, T., B. Nguyen, X. Zhang, and J. Yang. 1999. Architecture of a K^+ channel inner pore revealed by stoichiometric covalent modification. *Neuron*. 22:571–580. http://dx.doi.org/10.1016/S0896-6273(00)80711-4

Matsuda, H., A. Saigusa, and H. Irisawa. 1987. Ohmic conductance through the inwardly rectifying K channel and blocking by internal Mg^{2+}. *Nature*. 325:156–159. http://dx.doi.org/10.1038/325156a0

Matsuda, H., K. Oishi, and K. Omori. 2003. Voltage-dependent gating and block by internal spermine of the murine inwardly rectifying K^+ channel, Kir2.1. *J. Physiol.* 548:361–371. http://dx.doi.org/10.1113/jphysiol.2003.038844

Methfessel, C., V. Witzemann, T. Takahashi, M. Mishina, S. Numa, and B. Sakmann. 1986. Patch clamp measurements on Xenopus laevis oocytes: currents through endogenous channels and implanted acetylcholine receptor and sodium channels. *Pflugers Arch.* 407:577–588. http://dx.doi.org/10.1007/BF00582635

Noble, D. 1979. The Initiation of the Heart Beat. Oxford University Press. 200 pp.

Sigworth, F.J., and S.M. Sine. 1987. Data transformations for improved display and fitting of single-channel dwell time histograms. *Biophys. J.* 52:1047–1054.

Silberberg, S.D., and K.L. Magleby. 1997. Voltage-induced slow activation and deactivation of mechanosensitive channels in Xenopus oocytes. *J. Physiol.* 505:551–569. http://dx.doi.org/10.1111/j.1469-7793.1997.551ba.x

Stanfield, P.R., N.W. Davies, P.A. Shelton, M.J. Sutcliffe, I.A. Khan, W.J. Brammar, and E.C. Conley. 1994. A single aspartate residue is involved in both intrinsic gating and blockage by Mg^{2+} of the inward rectifier, IRK1. *J. Physiol.* 478:1–6.

Tao, X., J.L. Avalos, J. Chen, and R. MacKinnon. 2009. Crystal structure of the eukaryotic strong inward-rectifier K^+ channel Kir2.2 at 3.1 A resolution. *Science.* 326:1668–1674. http://dx.doi.org/10.1126/science.1180310

Terhag, J., N.A. Cavara, and M. Hollmann. 2010. Cave Canalem: how endogenous ion channels may interfere with heterologous expression in Xenopus oocytes. *Methods.* 51:66–74. http://dx.doi.org/10.1016/j.ymeth.2010.01.034

Vandenberg, C.A. 1987. Inward rectification of a potassium channel in cardiac ventricular cells depends on internal magnesium ions. *Proc. Natl. Acad. Sci. USA.* 84:2560–2564. http://dx.doi.org/10.1073/pnas.84.8.2560

Wible, B.A., M. Taglialatela, E. Ficker, and A.M. Brown. 1994. Gating of inwardly rectifying K^+ channels localized to a single negatively charged residue. *Nature.* 371:246–249. http://dx.doi.org/10.1038/371246a0

Xie, L.H., S.A. John, and J.N. Weiss. 2002. Spermine block of the strong inward rectifier potassium channel Kir2.1: dual roles of surface charge screening and pore block. *J. Gen. Physiol.* 120:53–66. http://dx.doi.org/10.1085/jgp.20028576

Xie, L.H., S.A. John, and J.N. Weiss. 2003. Inward rectification by polyamines in mouse Kir2.1 channels: synergy between blocking components. *J. Physiol.* 550:67–82. http://dx.doi.org/10.1113/jphysiol.2003.043117

Xie, L.H., S.A. John, B. Ribalet, and J.N. Weiss. 2005. Long polyamines act as cofactors in PIP2 activation of inward rectifier potassium (Kir2.1) channels. *J. Gen. Physiol.* 126:541–549. http://dx.doi.org/10.1085/jgp.200509380

Xie, L.H., S.A. John, B. Ribalet, and J.N. Weiss. 2008. Phosphatidyl-inositol-4,5-bisphosphate (PIP2) regulation of strong inward rectifier Kir2.1 channels: multilevel positive cooperativity. *J. Physiol.* 586:1833–1848. http://dx.doi.org/10.1113/jphysiol.2007.147868

Xu, Y., H.G. Shin, S. Szép, and Z. Lu. 2009. Physical determinants of strong voltage sensitivity of $K(^+)$ channel block. *Nat. Struct. Mol. Biol.* 16:1252–1258. http://dx.doi.org/10.1038/nsmb.1717

Yang, J., Y.N. Jan, and L.Y. Jan. 1995a. Control of rectification and permeation by residues in two distinct domains in an inward rectifier K^+ channel. *Neuron.* 14:1047–1054. http://dx.doi.org/10.1016/0896-6273(95)90343-7

Yang, J., Y.N. Jan, and L.Y. Jan. 1995b. Determination of the subunit stoichiometry of an inwardly rectifying potassium channel. *Neuron.* 15:1441–1447. http://dx.doi.org/10.1016/0896-6273(95)90021-7

Yang, X.C., and F. Sachs. 1990. Characterization of stretch-activated ion channels in Xenopus oocytes. *J . Physiol.* 431:103–122.

Yeh, S.H., H.K. Chang, and R.C. Shieh. 2005. Electrostatics in the cytoplasmic pore produce intrinsic inward rectification in kir2.1 channels. *J. Gen. Physiol.* 126:551–562. http://dx.doi.org/10.1085/jgp.200509367